Journal of Microwaves, Optoelectronics and Electromagnetic Applications, Vol. 22, No. 1, March 2023
DOI: http://dx.doi.org/10.1590/2179-10742023v22i1270773

Spectral Analysis of a SPR Sensor based on Multilayer Graphene in the Far Infrared Range

André Cruz[1], Wêndria Cunha[1], Tommaso Del Rosso[2], Victor Dmitriev[1], Karlo Costa[1]
[1]*Department of Electrical Engineering from Federal University of Pará, Brazil. E-mail: andcruz@ufpa.br, wendria.silva@tucurui.ufpa.br, victor@ufpa.br and karlo@ufpa.br*
[2]*Department of Physics from Pontifical Catholic University of Rio de Janeiro, Brazil. E-mail: tommaso@puc-rio.br.*

***Abstract*— In this paper, we present a spectral analysis of a Surface Plasmon Resonance (SPR) sensor based on multilayer graphene (MLG) operating as a terahertz refractometer. This device's structure is based on Kretschmann configuration, and the graphene layers are modeled as surface impedances with conductivity described by the Kubo model. The structure's electromagnetic response is obtained from the Generalized Coefficients Model, considering TM excitation performed in a frequency range from 1 to 4Thz. In this approach, we evaluate the sensor response for two, three, four and five layers of graphene, equally doped. To verify the effects of MLG doping, we varied the chemical potential by 0.35eV and 0.70eV. As a result, we present the plasmonic response of the device, verifying the operating frequency range for each case of multilayer graphene. In addition, the sensitivity, FWHM and Figure of Merit (FOM) are calculated to describe the sensor performance in each demonstrated case. From the results presented, we verified that the increase in doping reduces the sensitivity of the sensor, however, it improves its FOM. The validation of the proposed model was carried out from simulations in a software based on the Finite Element Method.**

***Index Terms*—** SPR sensor, Kretschmann configuration, Multilayer Graphene, Terahertz range .

I. Introduction

The research and development of new optical devices have been the subject of great attention in the last two decades. In this area of nanotechnology, we highlight the development of plasmonic devices based on noble metals for applications in biosensing, high-frequency modulation, optoelectronics, etc [1], [2]. The development of devices based on new plasmonic materials has been reported not only for high frequencies in the near-infrared (NIR), but also for the terahertz range in the far infrared (FIR) [3], [4], [5]. Among these materials, Graphene appears as a main element in plasmonic devices due to its extraordinary electromagnetic properties. Graphene is an allotrope of carbon that has a monoatomic layer with atoms covalently connected by strong $\sigma-$bonds, and weak $\pi-$bonds [6]. Since graphene has high electronic mobility and thickness of a single atomic layer, we can consider it as an approximately two-dimensional material, being modeled as a surface impedance described by Kubo's formula [7].

The plasmonic phenomenon is characterized by the material's collective oscillation of electron gas in the opposite phase to the incident electric field. In noble metals, this phenomenon arises at high frequencies in the optical range [2]. In contrast to this interaction, graphene is able to support TM plasmonic modes in the Terahertz range (FIR) [7], [8], [9], [10].

Brazilian Microwave and Optoelectronics Society-SBMO *received 4 Apr 2022; for review 11 Apr 2022; accepted 5 Dec 2022*
Brazilian Society of Electromagnetism-SBMag *ISSN 2179-1074*

Furthermore, the electrical conductivity of graphene can be tuned by applying an external polarizing electric field which, in turn, alters the chemical potential resulting in a dynamic doping of the material. This feature has allowed the development of new surface plasmon resonance (SPR) devices for sensing applications in the terahertz range [3], [4], [7]. A conventional SPR sensor in the Kretschmann configuration consists of a multilayer structure of dielectric substrates and graphene sheets, all deposited onto a dielectric prism, excited by an external electromagnetic source [11], [12]. The sensing process is based on the attenuated total reflection (ATR) angular interrogation method, where the plasmonic response of the sensor is a function of the dielectric sample RI [13], [14], [15].

In this paper, we present an analysis of a conventional SPR sensor in the Kretschmann configuration based on MLG. In this approach, the graphene layers are modeled as surface impedances equally doped with conductivities described by Kubo's formula. In the spectral analysis, we verified the frequency ranges for which sensors with two, three, four and fives layers of graphene operate with adequate performance. For the best values of sensitivity, FWHM, and FOM, we obtain the reflectivity curves as a function of the source incidence angle. The results were obtained considering two levels of chemical potential equally applied to the MLG structure, in order to demonstrate the effects of doping on the sensor performance parameters. To validate the results and the presented model, we compared the reflectivity curves with the results obtained from a numerical model developed in a software based on the Finite Element Method. For the case with $\mu_c = 0.35eV$ we found that the highest sensitivity was $S = 2.32°\text{RIU}^{-1}$ in the structure of four graphene layers, yet the highest FOM for this doping level was identified at the frequency $f = 2.45\text{THz}$ for five graphene layers. For the case with $\mu_c = 0.7eV$, the highest sensitivity was $S = 2.55°\text{RIU}^{-1}$ for two layers of graphene, and the best FOM was for five layers at frequency $f = 3.82\text{THz}$. Finally, we verified the magnetic field profiles in the structure considering the TM excitation performed at the appropriate plasmonic resonance angles.

II. Functional Description of the SPR Sensor

In Fig. 1 a functional description of the SPR Sensor in the Kretschmann configuration is shown.

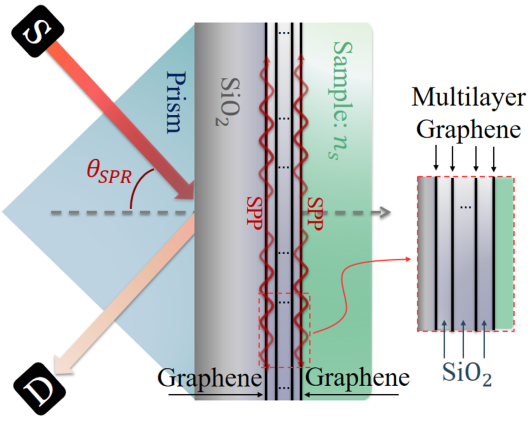

Fig. 1. Functional description of the MLG based SPR Sensor.

Fig. 1 shows a sensor structure, where the dialectric sample to be sensed is deposited above the MLG package, which in turn is above the SiO_2 substrate deposited on the glass prism. The excitation is carried out by an incident source (S) in the Prism region. Graphene layers are subjected to a polarization potential and, therefore, are able to support Surface Plasmon Polariton (SPP) modes.

Brazilian Microwave and Optoelectronics Society-SBMO *received 4 Apr 2022; for review 11 Apr 2022; accepted 5 Dec 2022*
Brazilian Society of Electromagnetism-SBMag

ISSN 2179-1074

In the SPR sensor of Fig. 1, when θ_i reaches a certain angle where all the radiation is transmitted to the MLG structure, we have what is known as the SPR condition, because of that, this angle is called θ_{SPR}. For small variations in the sample refractive index (RI), we have a change in the plasmonic angle, thus defining the sensing process. This process is often referred to as Attenuated Total Reflection (ATR) angular interrogation method, being performed by a detector (D) of the reflected signal [11], [13]. For the electromagnetic description in the sensor structure, we propose to use a mathematical model based on the Generalized Reflection Coefficient, with TM excitation, as this is the most efficient type to obtain the plasmonic response of the graphene-based sensor.

III. Equivalent Electromagnetic Model

The main point in spectral analysis of the Kretschmann configuration sensor is to determine the reflected wave's behavior, measured by detector, as a function of the sensor's functional parameters: operating frequency, geometry, impedances; and as a function of the range of sensed samples. Considering that the excitation is performed by a TM-plane wave with amplitude A_1, we basically need to determine the generalized reflection coefficient $\tilde{r}_{12}^{TM}$ as a function of all these variables. Fortunately, the solution to this problem can be determined by the Generalized Coefficients Method, which describes the transverse magnetic field in the multilayer structure [7], [13], [16].

In Fig. 2 the equivalent electromagnetic model of the SPR sensor in the Kretschmann configuration is illustrated.

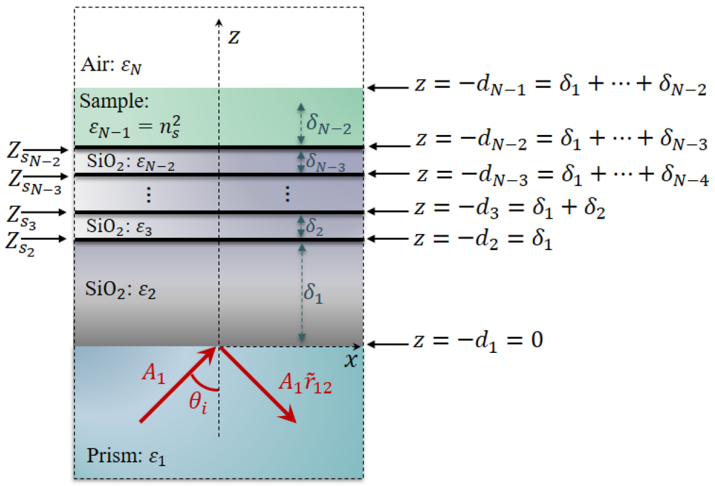

Fig. 2. Equivalent electromagnetic model of the MLG based SPR sensor.

In Fig. 2, the structure has N layers: Prism/ SiO_2 substrate/ MLG/ Sample/ Air, where MLG package has $N-4$ SiO_2 dieletric separators, interfaced by $N_g = N - 4 + 1$ surface impedances Z_s of graphene. Therefore, the number of layers N in the sensor directly depends on the number of impedances N_g in the MLG packet, for example: 1 impedance (SLG): $N = 4$; 2 impedances (DLG): $N = 5$; 3 impedances (TLG): $N = 6$; 4 impedances (QLG): $N = 7$, and so on. The structure is non-magnetic ($\mu_r = 1$), being basically characterized by the relative permitivity (ε_r) of each medium.

Distributing the multilayers along z-axis, the interfaces are located at $z = -d_1$, $z = -d_2$, ..., $z = -d_{N-1}$. The solution to TM excitation problem in the multilayer structure can be achieved by applying boundary conditions of the continuous tangential fields in $z = -d_1$ and $z = -d_{N-1}$ interfaces, and surface impedance condition in the remaining interfaces [7], [17].

ISSN 2179-1074

According to the geometric system described in Fg. 2, the transverse magnetic field in the i medium can be described by combination of an incident wave with amplitude A_i and another resulting from multiple reflections, with amplitude $A_i\tilde{r}_{i,i+1}^{TM}$, as described by [7]:

$$\mathbf{H}_i^{TM}(x,z) = A_i\left[e^{-jk_{zi}z} + \tilde{r}_{i,i+1}^{TM}e^{2jk_{zi}d_i}e^{jk_{zi}z}\right]e^{-jk_x x}(-\mathbf{a}_y) \tag{1}$$

where k_x and k_{zi} are the components of the propagation constant $|\mathbf{K}_i| = \omega\sqrt{\varepsilon_i\mu_i} = \sqrt{k_{zi}^2 + k_x^2}$ in the medium $i = 1, 2, ..., N$. Using Ampere's law, we can also define the electric field in N media: $\mathbf{E}_i^{TM} = (1/j\omega\varepsilon_i)\nabla \times \mathbf{H}_i^{TM}$.

To determine the generalized reflection and transmission coefficients, we need to apply the conditions of continuity of the tangential electric field: $\mathbf{a}_z \times \left[\mathbf{E}_{i+1}^{TM} - \mathbf{E}_i^{TM}\right] = \mathbf{0}$ and discontinuity of the magnetic field: $\mathbf{a}_z \times \left[\mathbf{H}_{i+1}^{TM} - \mathbf{H}_i^{TM}\right] = \mathbf{J}_{Si}$, according to the impedance condition: $\mathbf{J}_{Si} = \sigma_{gi}\mathbf{E}_{tangential}^{TM}$, where $\sigma_{gi} = Z_{Si}^{-1}$ is the surface conductivity of graphene at the interface between media $i+1$ and i . From this method, the generalized reflection coefficient in the medium i is defined in (2).

$$\tilde{r}_{i,i+1}^{TM} = \frac{R_{i,i+1}^{TM} + [T_{i,i+1}^{TM} - R_{i,i+1}^{TM}]\tilde{r}_{i+1,i+2}^{TM}e^{-2jk_{z_{i+1}}(d_i - d_{i+1})}}{1 + [T_{i,i+1}^{TM} - 1]\tilde{r}_{i+1,i+2}^{TM}e^{-2jk_{z_{i+1}}(d_i - d_{i+1})}} \tag{2}$$

The Fresnel coefficients of TM mode, considering the existence of an impedance Z_{S_i} between the media i and $i+1$, are given by [7], [16]:

$$R_{i,i+1}^{TM} = \frac{\varepsilon_{i+1}k_{z_i} - \varepsilon_i k_{z_{i+1}} + k_{z_i}k_{z_{i+1}}(\omega Z_{S_i})^{-1}}{\varepsilon_{i+1}k_{z_i} + \varepsilon_i k_{z_{i+1}} + k_{z_i}k_{z_{i+1}}(\omega Z_{S_i})^{-1}} \tag{3}$$

$$T_{i,i+1}^{TM} = \frac{2\varepsilon_{i+1}k_{z_i}}{\varepsilon_{i+1}k_{z_i} + \varepsilon_i k_{z_{i+1}} + k_{z_i}k_{z_{i+1}}(\omega Z_{S_i})^{-1}} \tag{4}$$

In the medium $i = N$ the generalized coefficient $\tilde{r}_{N,N+1}^{TM} = 0$, and therefore, in the medium $i = N-1$ we have $\tilde{r}_{N-1,N}^{TM} = R_{N-1,N}^{TM}$. In medium 1 the incident wave has amplitude $A_1 = H_0 e^{-jk_{z_1}d_1}$ adjusted by the field H_0 of the external excitation. The amplitude of A_i in the media $i = 2, ..., N$ is defined by:

$$A_i = A_1\frac{e^{jk_{z_1}d_1}}{e^{jk_{z_i}d_{i-1}}}\tilde{t}_{1i}^{TM} \tag{5}$$

where $\tilde{t}_{1i}^{TM}$ is the generalized transmission coefficient:

$$\tilde{t}_{1i}^{TM} = \prod_{g=1}^{i-1}\frac{T_{g,g+1}^{TM}e^{-jk_{z_g}(d_{g-1} - d_g)}}{1 + [T_{g,g+1}^{TM} - 1]\tilde{r}_{g+1,g+2}^{TM}e^{-2jk_{z_{g+1}}(d_g - d_{g+1})}} \tag{6}$$

The incidence angle θ_i defines the propagation constant in x-direction in all media, by $k_x = |\mathbf{K}_1|\sin\theta_i$, and thus, the propagation constant in z-direction by $k_{zi} = \sqrt{\omega^2\varepsilon_i\mu_i - k_x^2}$.

At $z = -d_1$ and $z = -d_{N-1}$ interfaces there are no surface impedances of graphene, so we can simply make $Z_{S_1} \approx \infty$ and $Z_{S_{N-1}} \approx \infty$, which indicates null conductivity at these interfaces. In the MLG package the impedances $Z_{S_i} = 1/\sigma_{g_i}$ $(i = 2 : N-2)$ have conductivity described by the intraband term of Kubo's Formula [7]:

$$\sigma_g(\omega) = \frac{\sigma_0}{\pi}\frac{4/\hbar}{j\omega + \tau^{-1}}\left[\mu_c + 2k_B T\ln\left(1 + e^{-\mu_c/k_B T}\right)\right] \tag{7}$$

where $\sigma_0 = e^2/4\hbar$ is the HF conductivity, e is the electron charge, $\hbar$ is the reduced Plank constant, k_B is the Boltzmann constant, and v_F is the Fermi speed, all for Temperature $T = 300K$.

Brazilian Microwave and Optoelectronics Society-SBMO *received 4 Apr 2022; for review 11 Apr 2022; accepted 5 Dec 2022*
Brazilian Society of Electromagnetism-SBMag *ISSN 2179-1074*

In Fig. 3 shows the real and imaginary parts of the conductivity (7) in the range from 1 to 4THz, considering three levels of doping.

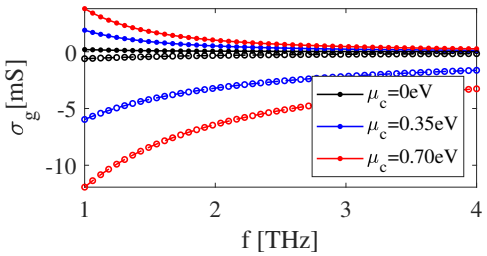

Fig. 3. Intraband term of the surface conductivity of graphene. Line with dots: $\Re\{\sigma_g\}$, with circles: $\Im\{\sigma_g\}$. Black: $\mu_c = 0eV$, blue: $\mu_c = 0.35eV$, red: $\mu_c = 0.70eV$.

The performance of SPR sensors depends on three main parameters: sensitivity, detection accuracy and quality factor (figure of merit) [1]. All these characteristic parameters must have high values in order to allow a good performance of the SPR sensor.

For a sensor that aims to evaluate changes in the RI of an external medium to its structure, the sensitivity parameter (Bulk Sensitivity) is defined as the ratio between the variation of the resonance angle ($\Delta\theta_{SPR}$) and the variation of the refractive index of the sample (Δn_s, where $n_s = \varepsilon_s^2$). Sensitivity S has dimension $^\circ RIU^{-1}$, being expressed by [1]:

$$S = \lim_{\Delta n_s \to 0} \frac{\Delta\theta_{SPR}}{\Delta n_s} \tag{8}$$

In sensors based on the angular interrogation method, another important factor is Full Width Half at Maximum. The smaller the FWHM, the more accurate the sensor, for this reason, we define the quality factor, or figure of merit, with dimension RIU^{-1}, by:

$$\text{FOM} = \frac{S}{\text{FWHM}} \tag{9}$$

FWHM is a parameter of a curve or function referring to its notch. In the graph of Reflectance versus angle of incidence, the FWHM is measured from the difference between the angles that produce half of the minimum reflectance. From this we can define the detection accuracy, by:

$$\text{DA} = \frac{\Delta\theta_{SPR}}{\text{FWHM}} \times 100\% \tag{10}$$

For a small change in sample RI, a DA of 100% indicates that the $\Delta\theta_{SPP}$ change is equivalent to the FWHM of the sensor response.

IV. Results

From the analytical model presented in the previous section, a code MATLAB®was written to simulate the structure with $N_g = 2$ ($N = 5$), $N_g = 3$ ($N = 6$), $N_g = 4$ ($N = 7$) and $N_g = 5$ ($N = 8$) graphene layers. In these simulations we use the following relative permittivity: $\varepsilon_{r1} = 14$ (Dielectric Prism), $\varepsilon_{r2} = 4$ (SiO_2 substrate with thickness: $\delta_1 = 20\mu m$), $\varepsilon_{r3} = \ldots = \varepsilon_{r_{N-2}} = 4$ (SiO_2 dielectric separators, all with $\delta_2 = \ldots = \delta_{N-3} = 1\mu m$), $\varepsilon_{r_{N-1}} = n_s^2 = 2$ (Dielectric sample with: $\delta_{N-2} = 5\mu m$), $\varepsilon_{r_N} = 1$ outer layer of Air. To calculate Sensitivity, the RI of the sample was varied in $n_s = 1.31RIU$, $1.41RIU$ and $1.51RIU$ (variations around $\varepsilon_{r_{N-1}} = 2$). All impedances in MLG package were subjected to the same conductivity.

ISSN 2179-1074

It is already known that graphene has a plasmonic response in the far infrared range, however, we need to find out what the operating ranges are for the SPR sensor based on multilayer graphene, doped at a certain level of chemical potential. Fig. 4 shows the reflectivity $R = |\tilde{r}_{12}^{TM}|^2$ as a function of frequency f (Range from 1 to 4 THz) and the incidence angle θ_i (from 20° to 60°) for the cases $N_g = 2$, $N_g = 3$, $N_g = 4$ and $N_g = 5$, considering doping the MLG package at $\mu_c = 0.35eV$. In Fig. 5 a similar result is shown, considering the doping level of $\mu_c = 0.7eV$.

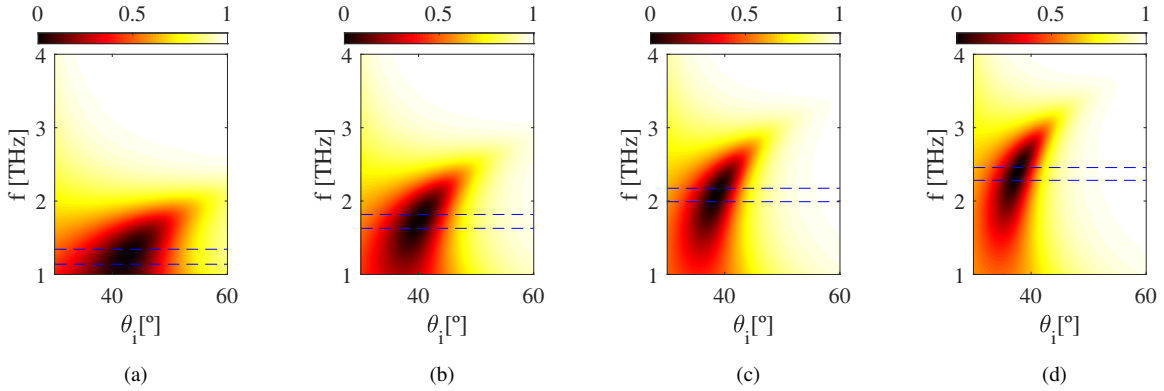

Fig. 4. $R = |\tilde{R}_{12}^{TM}|^2$ as a function of f and θ_i, for MLG package doped at $\mu_c = 0.35eV$ with: (a) $N_g = 2$, (b) $N_g = 3$, (c) $N_g = 4$ e (d)$N_g = 5$. Dashed blue lines delimit the $R < 1\%$ region.

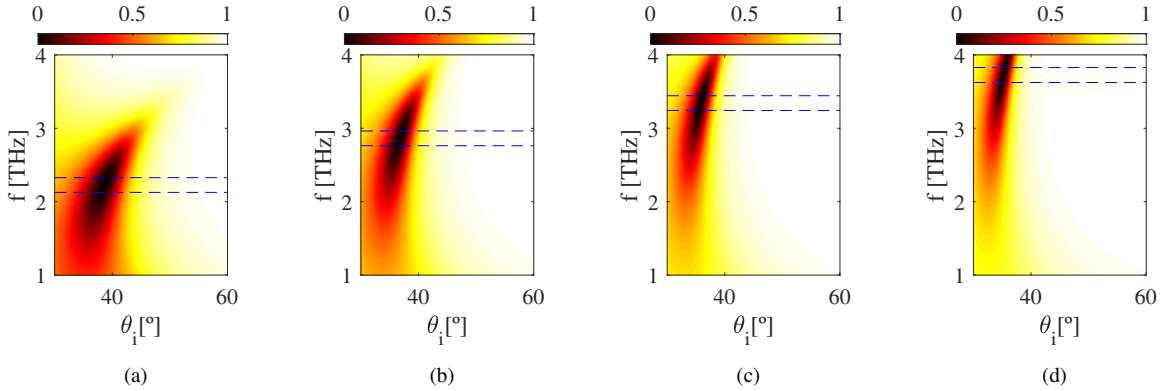

Fig. 5. $R = |\tilde{R}_{12}^{TM}|^2$ as a function of f and θ_i, for MLG package doped at $\mu_c = 0.70eV$ with: (a) $N_g = 2$, (b) $N_g = 3$, (c) $N_g = 4$ e (d)$N_g = 5$. Dashed blue lines delimit the $R < 1\%$ region.

From Fig. 4 and Fig. 5, we can verify that ATR region of the resonance angles is shifted depending on the number of graphene impedances in the MLG package, for higher frequencies with the increase of N_g. This frequency shift can be explained by the coupling between the individual resonances of the graphene impedances in the MLG package.

In Fig. 4 and Fig. 5, we also highlight the frequency bands for $|R| < 0.01$, delimiting the ATR region with a reflection of at most 1% of the incident wave. For the cases with doping $\mu_c = 0.35eV$ in Fig. 4, the frequency bands within delimited region are $f = 1.13$THz to 1.34THz for $N_g = 2$, $f = 1.62$THz to 1.81THz for $N_g = 3$, $f = 1.99$THz to 2.17THz for $N_g = 4$ and $f = 2.28$THz to 2.45THz for $N_g = 5$. As for the cases with doping $\mu_c = 0.7eV$ in Fig. 5, the frequency bands are $f = 2.12$THz to 2.32THz for $N_g = 2$, $f = 2.76$THz to 2.96THz for $N_g = 3$, $f = 3.24$THz to 3.44THz for $N_g = 4$ and $f = 3.62$THz to 3.82THz for $N_g = 5$.

In addition to the remarkable shift with increasing graphene impedances in the MLG package, we can also show that the increase in graphene doping shifts the ATR region of plasmonic response to higher frequencies. Another factor that draws attention to the cases with $\mu_c = 0.35eV$ is the decrease in bandwidth for ATR region with $R < 0.01$, falling from $\Delta f = 0.20\text{THz}$ in the case $Ng = 2$ to $\Delta f = 0.17\text{THz}$ in the case $N_g = 5$. However, cases with doping $\mu_c = 0.7eV$ showed bandwidths close to $\Delta f = 0.20\text{THz}$, regardless of the number of graphene impedances in the MLG package.

Now we need to evaluate the sensor performance parameters for each frequency range. In Fig. 6 sensitivity (8), FWHM and FOM (9) are shown for the four cases studied in Fig. 4 ($\mu_c = 0.35eV$), and for the four cases studied in Fig. 5 ($\mu_c = 0.7eV$).

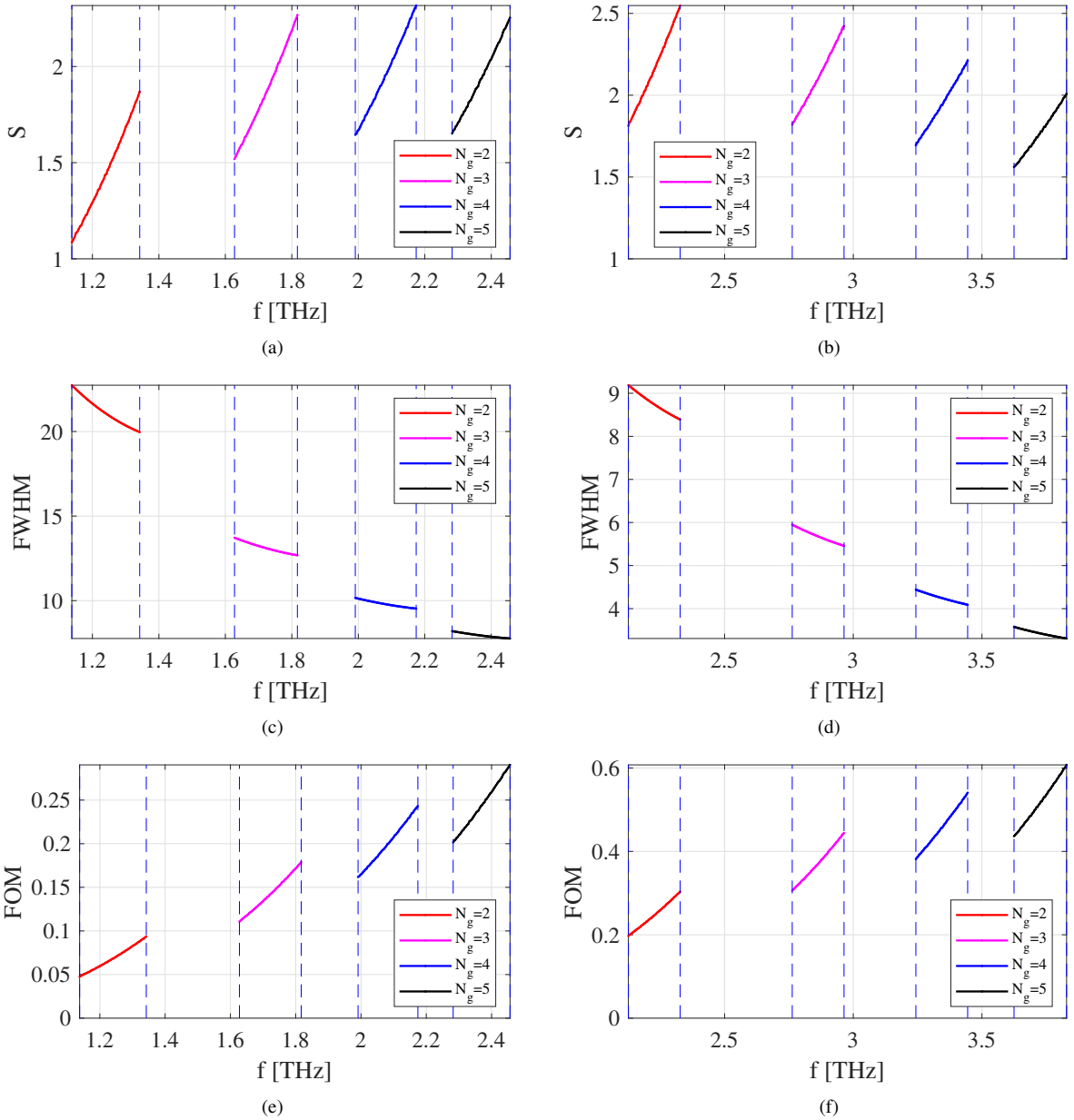

Fig. 6. SPR Sensor Quality Parameters. Sensitivity: (a) $\mu_c = 0.35eV$ and (b) $\mu_c = 0.70eV$; Full Width at Half Maximum: (c) $\mu_c = 0.35eV$ and (d) $\mu_c = 0.70eV$; Figure of Merit: (e) $\mu_c = 0.35eV$ and (f) $\mu_c = 0.70eV$. Blue dashed lines delimit the frequency ranges in which the reflectivity is at most 1%.

ISSN 2179-1074

For doping $\mu_c = 0.35eV$, the result with highest sensitivity was the case $N_g = 4$, with $S = 2.32°\text{RIU}^{-1}$ at frequency 2.17THz. Increasing the doping to $\mu_c = 0.7eV$, the highest sensitivity was obtained for $N_g = 2$, with $S = 2.55°\text{RIU}^{-1}$ at 2.12THz. From Fig. 6c and 6d, it is notable that the increase in the number of graphene layers results in a decrease in FWHM, thus resulting in an increase in FOM. From Fig. 6e and 6f, we verified that for both $\mu_c = 0.35eV$ and $0.70eV$ doping, for each case of N_g the highest FOM was presented by the highest frequency in each band.

From definition (10) we can also calculate the detection accuracy for each case of best FOM. The FOM then appears as a key parameter for comparison between the structures, indicating that, from the eight cases analyzed, the sensor based on five layers, equally doped with $0.70eV$, showed better performance parameters. The best FOM results in Fig. 6 are summarized in Table I and Table II.

TABLE I. PERFORMANCE PARAMETERS: RESULTS FOR BEST FOM OF CASES WITH DOPING $\mu_c = 0.35eV$

N_g	f[THz]	$S[°\text{RIU}^{-1}]$	FWHM[°]	FOM[RIU^{-1}]	DA[%]
2	1.34	1.86	19.96	0.09	1.86
3	1.81	2.26	12.68	0.17	3.57
4	2.17	2.32	9.53	0.24	4.87
5	2.45	2.25	7.76	0.29	5.81

TABLE II. PERFORMANCE PARAMETERS: RESULTS FOR BEST FOM OF CASES WITH DOPING $\mu_c = 0.70eV$

N_g	f[THz]	$S[°\text{RIU}^{-1}]$	FWHM[°]	FOM[RIU^{-1}]	DA[%]
2	2.32	2.55	8.38	0.30	6.07
3	2.96	2.43	5.45	0.44	8.90
4	3.44	2.21	4.09	0.54	10.82
5	3.82	2.00	3.30	0.60	12.11

Fig. 7 shows the reflectivity $R = |\tilde{r}_{12}^{TM}|$ for the four N_g values with the best FOM presented in Table I, while Fig. 8 shows $R = |\tilde{r}_{12}^{TM}|$ for the four N_g values with the best FOM shown in Table II.

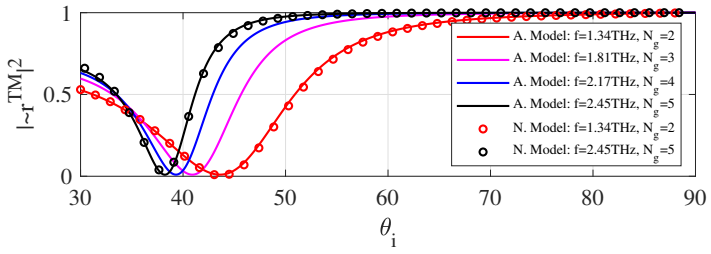

Fig. 7. Reflectivity for better FOM, with $\mu_c = 0.35eV$. Analytical models in solid lines, and numerical models in circles.

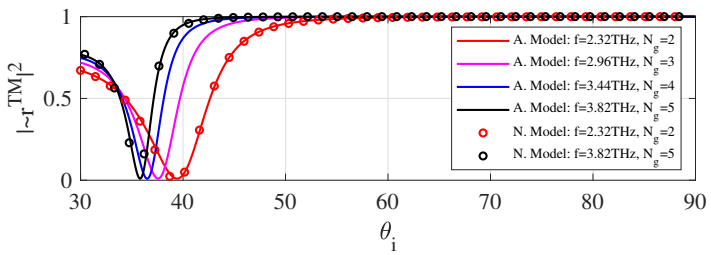

Fig. 8. Reflectivity for better FOM, with $\mu_c = 0.70eV$. Analytical models in solid lines, and numerical models in circles.

Brazilian Microwave and Optoelectronics Society-SBMO *received 4 Apr 2022; for review 11 Apr 2022; accepted 5 Dec 2022*
Brazilian Society of Electromagnetism-SBMag

ISSN 2179-1074

To validate the presented analytical model, a numerical model was prepared in the COMSOL Multiphysics®software to generate the reflectivity results for $N_g = 2$ and $N_g = 5$ cases, and they were compared with the analytical results in Fig. 7 for $\mu_c = 0.35eV$, and Fig. 8 for $\mu_c = 0.70eV$.

Comparing the analytical and numerical results for the extreme cases ($N_g = 2$ and $N_g = 5$), we verified a satisfactory correspondence between the models.

From Fig. 7 and Fig. 8, we also verified that the plasmonic resonance angle is shifted to the left when the number of graphene layers increases. For the cases studied in Fig. 7, SPR angles are: $\theta_{SPR} = 43.59°$ for $N_g = 2$, $\theta_{SPR} = 40.90°$ for $N_g = 3$, $\theta_{SPR} = 39.31°$ for $N_g = 4$ and $\theta_{SPR} = 38.22°$ for $N_g = 5$. For the cases studied in Fig. 8, SPR angles are: $\theta_{SPR} = 39.41°$ for $N_g = 2$, $\theta_{SPR} = 37.56°$ for $N_g = 3$, $\theta_{SPR} = 36.50°$ for $N_g = 4$ and $\theta_{SPR} = 35.81°$ for $N_g = 5$.

In Fig. 9, the profile of the transverse magnetic field ($\Re\{H_y(x,z)\}$) is shown for each plasmonic resonance angle obtained in the result of Fig. 7, while in Fig. 10 the field profiles are calculated for each plasmonic resonance angle obtained in the result of Fig. 8. Field graphs were generated in the $y = 0$ plane, which is the TM wave incidence plane.

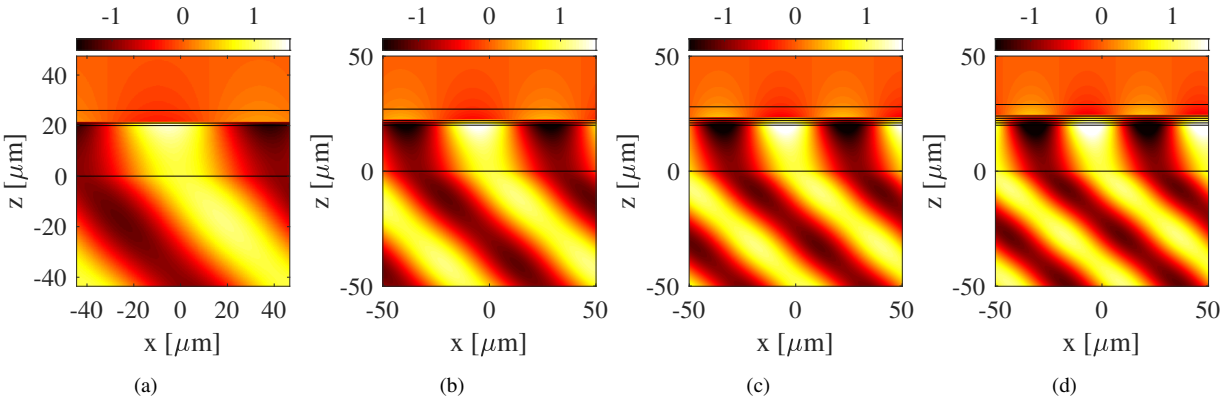

Fig. 9. $\Re\{H_y\}$ in the $y = 0$ plane, for MLG structure with doping $\mu_c = 0.35eV$. Excitation with: (a) $\theta_{SPR} = 43.59°$ for $N_g = 2$, (b) $\theta_{SPR} = 40.90°$ for $N_g = 3$, (c) $\theta_{SPR} = 39.31°$ for $N_g = 4$ and (d) $\theta_{SPR} = 38.22°$ for $N_g = 5$.

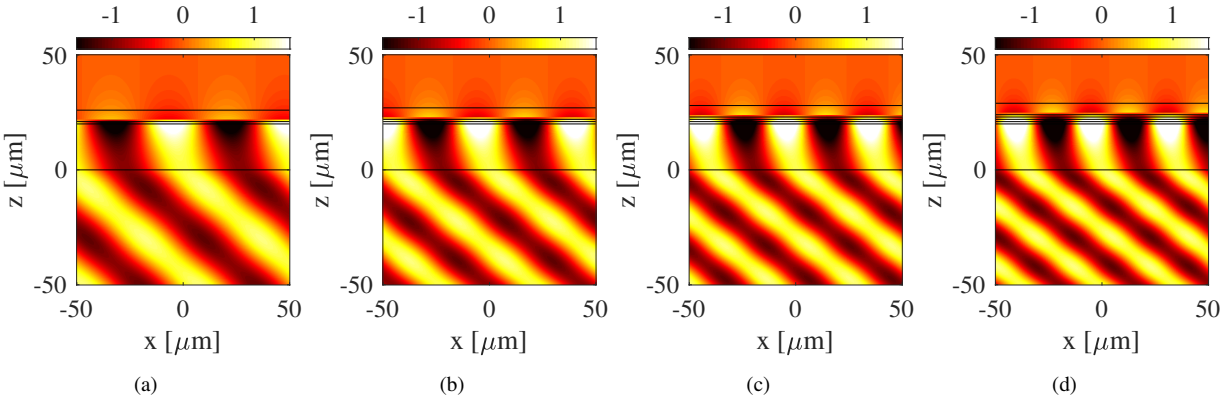

Fig. 10. $\Re\{H_y\}$ in the $y = 0$ plane, for MLG structure with doping $\mu_c = 0.70eV$. Excitation with: (a) $\theta_{SPR} = 39.41°$ for $N_g = 2$, (b) $\theta_{SPR} = 37.56°$ for $N_g = 3$, (c) $\theta_{SPR} = 36.50°$ for $N_g = 4$ and (d) $\theta_{SPR} = 35.81°$ for $N_g = 5$.

From Fig. 9 and Fig. 10, the appearance of SPP wave on the interfaces containing the surface impedances of the MLG packet is evident. Also note the minimal incident wave reflection ($\sim 1\%$).

ISSN 2179-1074

From the graphical results of the field profile, we verified that the enhancement of plasmonic resonance occurs in two situations, from Fig. 9 with increasing number of graphene layers, and comparing the results of Fig. 9 Fig. 10, with the increase in the chemical potential applied to the MLG package.

The results shown so far were obtained from simulations considering a dielectric sample with $\varepsilon_{r_{N-1}} = 2$ $(n_s = 1.41\text{RIU})$. It is important to highlight the nature of sensitivity as a function of the range of samples sensed. We can express the sensitivity as a linear approximation $S = S_0 + (dS/dn_s) \times n_s + ...$, and then perform an analysis on the variation of the sensor's quality parameters as a function of the RI of the sample. In Fig. 11 we show how S, FWHM and FOM vary as a function of n_s, for the two doping cases under analysis. In these results we highlight the values for $n_s = 1.41\text{RIU}$.

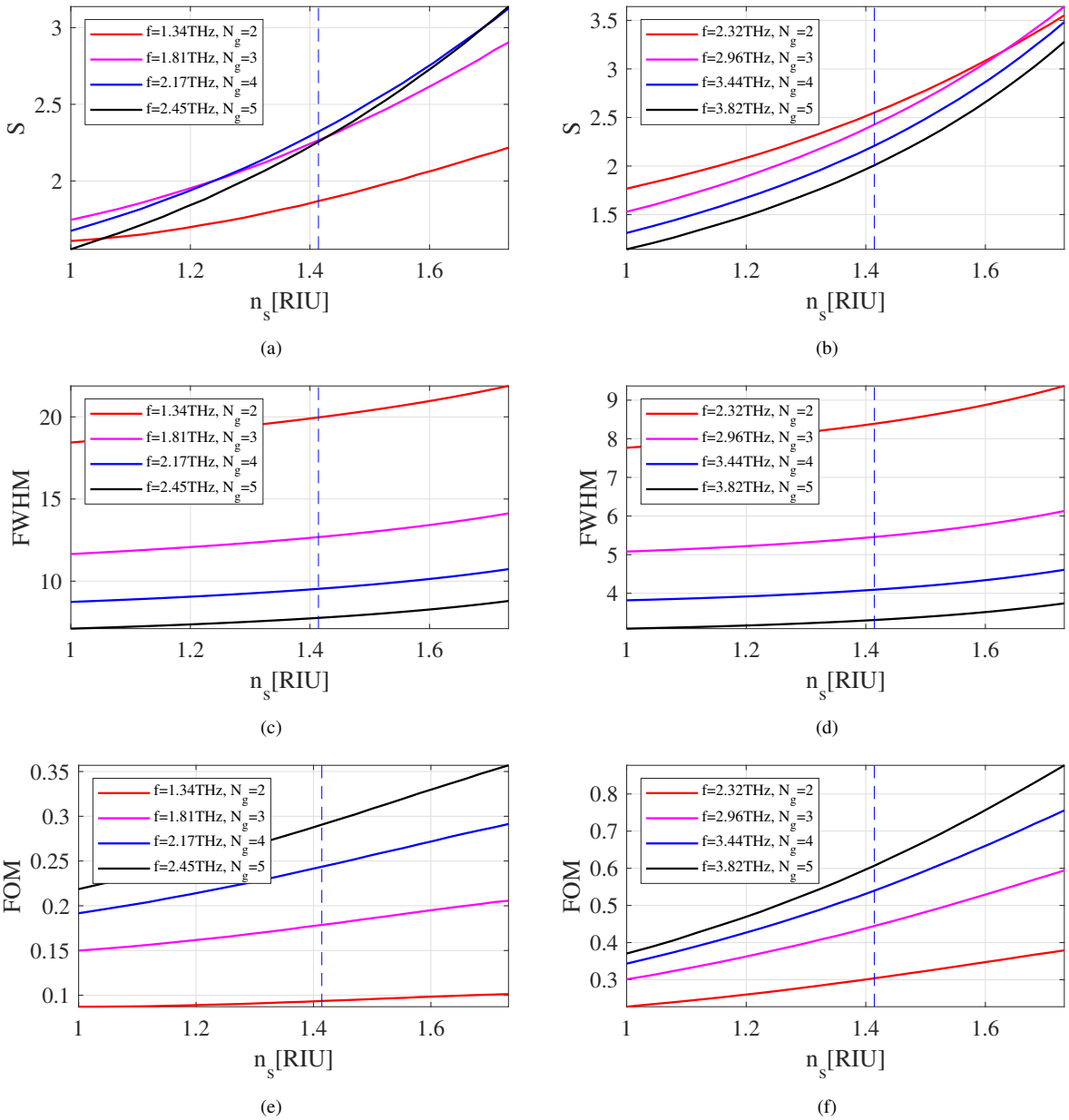

Fig. 11. SPR Sensor quality parameters as a function of the refractive index of the sample. Sensitivity: (a) $\mu_c = 0.35eV$ and (b) $\mu_c = 0.70eV$; Full Width at Half Maximum: (c) $\mu_c = 0.35eV$ and (d) $\mu_c = 0.70eV$; Figure of Merit: (e) $\mu_c = 0.35eV$ and (f) $\mu_c = 0.70eV$. Blue dashed lines indicates $n_s = 1.41\text{RIU}$ constant.

Brazilian Microwave and Optoelectronics Society-SBMO *received 4 Apr 2022; for review 11 Apr 2022; accepted 5 Dec 2022*
Brazilian Society of Electromagnetism-SBMag

ISSN 2179-1074

In order for the SPR sensor to display a "linear" response, it is necessary that dS/dn_s term and its superiors are very small, so the sensitivity is basically S_0. However, from the results in Fig. 11, it is evident that this is not the case. From Fig. 11, we verify that the response which shows uniform FOM is $N_g = 2$ with doping $0.35eV$ therefore, although the increase in the number of layers and doping of the MLG package improve the device's performance, we have an increase sensor response non-linearity.

V. CONCLUSIONS

In this work, a parametric analysis of the equivalent structure of a SPR sensor in the Kretschmann configuration based on Multilayer Graphene was presented. The simulations were carried out for four cases of SPR sensors, these with 2,3,4 and 5 layers of graphene, the latter modeled as surface impedances in an MLG package, equally doped at $0.35eV$ and $0.7eV$. For each case, we verified the terahertz frequency ranges of operation, where the sensor can demonstrate a reflection of at most 1% of the incident wave, during the ATR process.

The simulations were carried out using optimized codes in MATLAB software, being written from the definition of Generalized Coefficients Model for TM excitation in N layers, considering the existence of surface impedances at the interfaces between media. It is worth noting that the model in question provides a great theoretical basis for the study of multilayer devices with excitation from nearby sources, since in these cases, the electric and magnetic field distributions can be expressed by the linear combination of TM and TE waves with multiple propagation constants, similar to that described in full-wave solutions by Green's functions.

For the MLG package doped with $\mu_c = 0.35eV$, it was found that the best sensitivity was presented for $N_g = 4$ case, however, $N_g = 5$ structure showed better performance parameters: $S = 2.25°\mathrm{RIU}^{-1}$, $\mathrm{FOM} = 0.29\mathrm{RIU}^{-1}$ and $\mathrm{DA} = 5.81\%$. Increasing the doping to $\mu_c = 0.75eV$, it was verified that the best sensitivity was presented for $N_g = 2$, even so, the best performance parameters were presented by the structure $N_g = 5$: $S = 2.00°\mathrm{RIU}^{-1}$, $\mathrm{FOM} = 0.60\mathrm{RIU}^{-1}$ and $\mathrm{DA} = 12.11\%$. So, in terms of performance, we found that the higher the doping and the number of layers of the device, the better the performance.

However, this increase in doping and in the number of layers in the MLG package ends up introducing a less and less linear response as a function of a range of dielectric samples. For future work, it is proposed to investigate ways to maintain the high performance of the SPR sensor based on MLG, reducing the nonlinear dS/dn terms of the sensor response.

ACKNOWLEDGMENTS

The authors thank the members of the Nanoelectronics and Nanophotonics Laboratory from UFPA (NANOTIBO-UFPA), The Laboratory of Synthesis and Laser Characterization of Nanomaterials (NanoLaser-Lab) from Department of Physics of PUC-Rio, and CAPES-BRAZIL (Coordenação de Aperfeiçoamento de Pessoal de Nível Superior).

  ISSN 2179-1074

REFERENCES

[1] S. Singh, P. K. Singh, A. Umar, P. Lohia, H. Albargi, L. Castañeda, and D. Dwivedi, "2d nanomaterial-based surface plasmon resonance sensors for biosensing applications," *Micromachines*, vol. 11, no. 8, p. 779, 2020.

[2] S. A. Maier *et al.*, *Plasmonics: fundamentals and applications*. Springer, 2007, vol. 1.

[3] Y. Li, K. Tantiwanichapan, A. K. Swan, and R. Paiella, "Graphene plasmonic devices for terahertz optoelectronics," *Nanophotonics*, vol. 9, no. 7, pp. 1901–1920, 2020.

[4] Y. Xiang, J. Zhu, L. Wu, Q. You, B. Ruan, and X. Dai, "Highly sensitive terahertz gas sensor based on surface plasmon resonance with graphene," *IEEE Photonics Journal*, vol. 10, no. 1, pp. 1–7, 2017.

[5] N. Kakenov, M. S. Ergoktas, O. Balci, and C. Kocabas, "Graphene based terahertz phase modulators," *2D Materials*, vol. 5, no. 3, p. 035018, 2018.

[6] H.-S. P. Wong and D. Akinwande, *Carbon nanotube and graphene device physics*. Cambridge University Press, 2011.

[7] P. A. D. Gonçalves and N. M. Peres, *An introduction to graphene plasmonics*. World Scientific, 2016.

[8] T. Zhang, L. Chen, B. Wang, and X. Li, "Tunable broadband plasmonic field enhancement on a graphene surface using a normal-incidence plane wave at mid-infrared frequencies," *Scientific Reports*, vol. 5, no. 1, pp. 1–8, 2015.

[9] M. Aldrigo, M. Dragoman, A. Costanzo, and D. Dragoman, "Graphene as a high impedance surface for ultra-wideband electromagnetic waves," *Journal of Applied Physics*, vol. 114, no. 18, p. 184308, 2013.

[10] R.-B. Hwang, "A theoretical design of evanescent wave biosensors based on gate-controlled graphene surface plasmon resonance," *Scientific reports*, vol. 11, no. 1, pp. 1–10, 2021.

[11] Y. Huang, S. Zhong, H. Yao, and D. Cui, "Tunable terahertz plasmonic sensor based on graphene/insulator stacks," *IEEE Photonics Journal*, vol. 9, no. 1, pp. 1–10, 2017.

[12] P. Kumar, A. K. Sharma, and Y. K. Prajapati, "Graphene-based plasmonic sensor at thz frequency with photonic spin hall effect assisted by magneto-optic phenomenon," *Plasmonics*, pp. 1–7, 2022.

[13] J. S. Costa, Q. Zaman, K. Q da Costa, V. Dmitriev, O. Pandoli, G. Fontes, and T. Del Rosso, "Limits of the effective medium theory in particle amplified surface plasmon resonance spectroscopy biosensors," *Sensors*, vol. 19, no. 3, p. 584, 2019.

[14] T. Del Rosso, Q. Zaman, M. Cremona, O. Pandoli, and A. Barreto, "Spr sensors for monitoring the degradation processes of eu (dbm) 3 (phen) and alq3 thin films under atmospheric and uva exposure," *Applied Surface Science*, vol. 442, pp. 759–766, 2018.

[15] A. Cruz, Y. Gomes, W. Cunha, T. Del Rosso, V. Dmitriev, and K. Costa, "Spectral analysis of a multilayer graphene plasmonic sensor operating in far infrared," *2021 SBMO/IEEE MTT-S International Microwave and Optoelectronics Conference (IMOC)*, pp. 1–3, 2021.

[16] W. Chew, *Waves and fields in inhomogeneous media: IEEE*. Press, New York, 1990.

[17] A. Cruz, K. Costa, V. Dmitriev, N. Souza, Q. Zaman, and T. Del Rosso, "Electromagnetic model of a nanodipole array above a double-layer graphene by periodic green's function," *IET Microwaves, Antennas & Propagation*, vol. 14, no. 15, pp. 2088–2096, 2020.

Brazilian Microwave and Optoelectronics Society-SBMO *received 4 Apr 2022; for review 11 Apr 2022; accepted 5 Dec 2022*
Brazilian Society of Electromagnetism-SBMag *ISSN 2179-1074*